Polymer Testing 92 (2020) 106851

Contents lists available at ScienceDirect

Polymer Testing

journal homepage: http://www.elsevier.com/locate/polytest

Investigating electric field induced molecular distortions in polypropylene using Raman spectroscopy

Marleen Vetter *, Matthew J.F. Healy, David W. Lane

Cranfield Forensic Institute, Cranfield University, Defence Academy of the United Kingdom, Shrivenham, Swindon, SN6 8LA, UK

ARTICLE INFO

Keywords:
Polypropylene
Raman spectroscopy
Principal component analysis
Electric field stress

ABSTRACT

Polymeric electric insulators are an integral part of many electronic circuits and systems. Changes induced by an electric field can affect various mechanisms; including electrical polarisation and electromechanical properties. Changes in the dielectric material can be tracked using spectroscopic methods. This study has shown that analysing polypropylene under electric field stress using Raman spectroscopy in combination with principal component analysis allows small changes in the non-crystalline phase to be identified. We have observed that for polypropylene, vibrational motion and changes in conformation occur mostly within the tie molecules connecting the overall cluster network. Amorphous molecular chains in the spherulites were also found to orient and form into a smectic mesophase. These electromechanical changes at the micro- and macromolecular level were found to be generally reversible once the stress is removed. However, with increased aging, these changes may lead to adverse structural changes and thus, in the future, this information may be used to inform faults and defect detection within polymeric dielectric materials.

1. Introduction

Polymeric electrical insulators are used in a variety of electronic systems. Their response to stress, as induced by an electric field, is a major factor for the material's functionality and longevity. Electric field induced changes such as sub-nanometre displacements as well as more apparent changes on the micrometre scale within the lamellar and crystal clusters can affect various mechanisms; including electrical polarisation and electromechanical properties. The stress may also induce phase transitions, which in turn could impact electrical loss, operating frequency range and the voltage limit of electrical devices [1–3].

Polymers such as polypropylene (PP) are frequently used as electric insulators, for example in capacitors. PP is a stereo-regular polymer, with a hydrocarbon backbone consisting of carbon-carbon single bonds with pendant methyl groups arranged along one side of the polymer chain. PP can be found in a variety of different polymorphic forms: isotactic, syndiotactic and atactic. Polypropylene used in capacitor applications is isotactic (iPP), with a 2–3% atactic portion (aPP). Several different crystalline phases have been identified in iPP, referred to as the monoclinic α-phase, trigonal β-phase and orthorhombic γ-phase, as well as a smectic mesophase. Their crystalline structures have a common helical conformation of their polymer chains but differ in relative ordering and positioning of the helical chains [4–6].

Little research has been done regarding the reversible electric field stress within the initial elastic strain region, where strain is almost proportional to the applied stress and deformation is believed to be homogeneous. Here, the material recovers to its original state after the stress is removed [7]. Characterising the molecular orientation and morphological structure as well as the response of the supramolecular morphology to deformation processes such as electric field stresses has gained considerable interest over the last few years, especially when investigating capacitor materials such as ceramics and polymers [8].

Optical spectroscopy has previously been used to study mechanical stresses in semi-crystalline materials such as polymers, and several Raman bands have been shown to be especially sensitive to stress [9–15]. Electric field stress in particular has been shown to affect both the profile and the position of the spectral peaks; however, profile changes are usually evident only for uneven stress distributions, and usually only wavenumber shifts are exploited [16].

Raman spectroscopy is a technique based on inelastic scattering of monochromatic light, using the shift in frequency of the photons in comparison to the original monochromatic frequency to identify material or material constituents. Using this, the Raman effect provides

* Corresponding author.
E-mail address: m.vetter@cranfield.ac.uk (M. Vetter).

https://doi.org/10.1016/j.polymertesting.2020.106851
Received 1 June 2020; Received in revised form 24 August 2020; Accepted 4 September 2020
Available online 13 September 2020

information regarding, long range crystal structure, crystal orientation, temperature and mechanical strain among others. Strain in a material generally induces shifts in vibrational frequencies. Examining the nature of the vibrations and interatomic potentials can reveal local stress/strain distributions. The electronic and atomic states will be modified due to the stress, changing the scattering cross-section of electromagnetic radiation and the splitting of degeneracies of phonons, making Raman spectroscopy a good tool to probe materials under electric field stress [16,17]. There are two mechanisms by which an electric field can affect the Raman spectrum of a dielectric: atomic displacement and the Franz-Keldysh mechanism within the dielectric [18,19]. Since domain structure does not only depend on the electric field, but also on the individual stress state of a particular sample, it can be said that each specimen will most likely produce a unique Raman spectrum which characterises its domain distribution and redistribution [20]. Yet, few investigations have focused on a static electric field stress applied to polymeric materials.

In this study we aim to investigate the response of the supramolecular morphology to an electric field under normal environmental conditions, and to understand the induced deformation processes within bulk iPP. This will be achieved by studying wavenumber shifts and profile effects from conventional Raman spectroscopy.

2. Materials

Homopolymer polypropylene blocks were purchased from Direct Plastics (Sheffield, UK) and cut into the required size (Fig. 1a and b). Using X-ray diffraction (XRD) measurements (2 theta range of 5-60°, voltage 40 kV, current 40 mA) the polymer blocks were determined to consist mainly of α-iPP, with a small atactic component. The electrodes were made of copper, and had insulated cables attached using tin solder before being inserted into machined holes in the PP blocks. This resulted in a tight fit that held the electrodes firmly in place. A Philip Harris stabilized DC power supply was used to apply a constant bias of up to 5 kV across the electrodes during some of the measurements. The output resistance of the power supply and the capacitance of the PP blocks and their cables meant that the high voltage bias stabilized within a few seconds, and before any spectra were recorded.

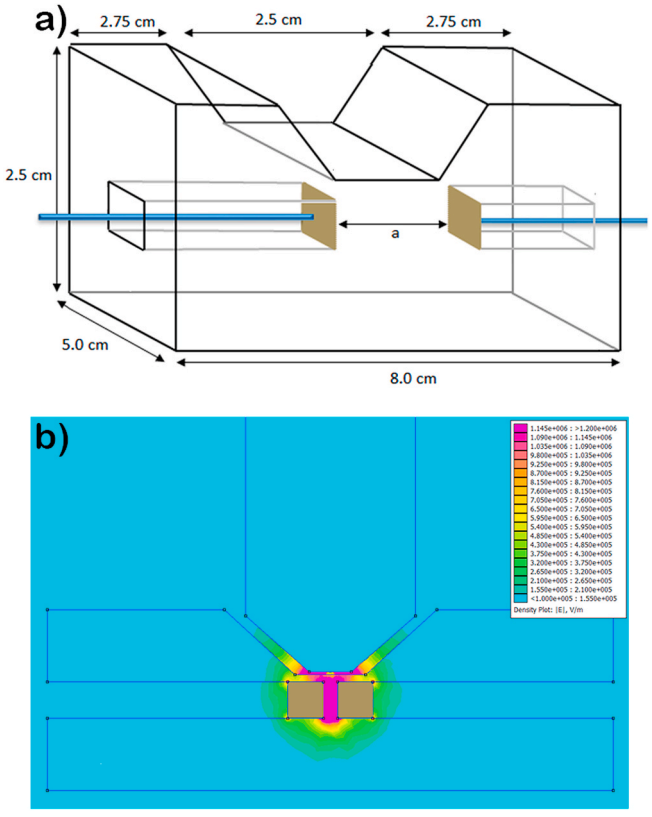

Fig. 1. Illustration of PP blocks used for analysis. a) Model of PP block used for Raman Spectroscopy, **'a'** corresponding to 2 mm and 5 mm for the distance between electrodes of both type of blocks b) FEMM model of Raman block and its electric field strength with an applied voltage of 5 kV.

3. Experimental

Raman analysis was performed on a Horiba Jobin Yvon LabRAM 300 microscope with a 300 mm focal length spectrometer (grating 1800 lines per mm) equipped with a BX41 confocal microscope attachment from Olympus and fitted with a 532 nm laser from Laser Quantum. The confocal hole size was 1000 μm and the spectrometer slit set to 100 μm. A 50× objective was used for all spectroscopic analysis (NA 0.75, working distance ~0.5 mm). Settings such as scan range, laser power (10–0.1 mW) and exposure time were optimised for each analysis but were usually set around 10 mW for 15 s. As a spike filter for cosmic rays, each spectrum was recorded twice. Instrument calibration was performed by measuring the Raman peak position of a standard silicon wafer before measurements.

Tests on the stability of PP were performed prior to the analysis and showed that laser-induced heating due to the power density used was not an issue. Further, the possibility of orientation within the sample influencing the Raman spectra was investigated but no significant influence was found. Therefore, it was assumed that the directionality within the sample, and the effect the inherent polarisation of the conventional Raman would have, are negligible.

Raman spectra were recorded over the range of 50–3500 cm^{-1} to include the CH stretching region and lower lying wavenumbers within the fingerprint region. In total, 930 Raman spectra were recorded, 266 with the sample electrically biased (i.e. charged) and 664 without an electrical bias (i.e. non-charged).

Two sample blocks with different electric field capabilities were constructed by changing the distance ***'a'*** between the electrodes. For the block with a distance ***'a'*** of 5 mm, 16 sites were measured, for the block with a distance ***'a'*** of 2 mm 15 different sites between the electrodes were measured, and the site noted as either close to the positive or negative electrode or within the middle of the block.

Seven spectra were measured at each site per electric field applied. The voltage was applied over the time of the spectral scan. Thereafter it was turned off, the output continuously monitored, and a zero applied voltage measurement performed. Initial tests showed that the baseline of the first Raman spectra collected from a sample site was higher than those from subsequent spectra collected from the same area. Subsequent spectra showed a consistent baseline and no reversibility, or hysteresis in the effect, could be observed. Therefore, this was believed to be caused by surface residue that was removed by the laser, rather than photo-induced bleaching. Consequently, the first spectrum of every analysis without applied electric field was discarded. After this, six further spectra were collected. These were arranged in pairs, either with or without applied electric field and their averages calculated. The averaged spectra were used to determine the difference (D) and residual (R) for each run (Equation (1) and (2)). The order of which the electric field and zero measurements were taken was randomised to avoid any systematic drift in the instrumentation.

$$D = (Raman\ Intensity)_{zerofield} - (Raman\ Intensity)_{E-Field} \quad \text{(Equation 1)}$$

$$R = \frac{(Raman\ Intensity)_{zerofield} - (Raman\ Intensity)_{E-Field}}{(Raman\ Intensity)_{zerofield}} \quad \text{(Equation 2)}$$

All spectra were recorded and initially processed using the LabRAM associated LabSPEC software (Version 6.4.4.16, 2014).

The data was then normalised, averaged, and the residuals and

differences calculated using a Matlab© (R2019b) script. Residuals and differences were calculated to avoid giving weight to analysis bias and inherent instrument effects in the statistical analysis. A Matlab© script was then used to perform principal component analysis (PCA). Peak positions were determined by fitting a Gauss-Lorentzian profile for symmetrical and a Pearson type IV profile for asymmetrical bands to the Raman spectra. With this, the resulting peak position considered both spectral and intensity error of the spectrometer and an accuracy of around ±0.01 cm^{-1} could be achieved. Raman group wavenumbers were assigned using text book literature [16,21].

Modelling of the electric field strength in the devices was performed using Finite Element Method Magnetics (FEMM) 4.2 [22]. An applied electric field higher than 2×10^6 Vm^{-1} could not be achieved as otherwise electric field strength between the sample and the objective of the Raman microscope could reach the breakdown strength of air (Fig. 1 c).

4. Results

The area where the spectra was taken from (either near an electrode or within the middle) had no observable effect on the results.

As no consistent changes were identified between the raw charged and non-charged datasets by visual observation, difference and residual analysis was performed as they accommodate inherent background.

However, when investigating the changes in charged and non-charged PP by observing the difference plots, some Raman peaks stand out (Table 1). For difference plots, these include bands at 401 cm^{-1}, 813/845 cm^{-1}, 977 cm^{-1}, 1156/1171 cm^{-1}, 1332 cm^{-1}, 1439/1461 cm^{-1}, 2841 cm^{-1}, 2868/2885/2906 cm^{-1}, 2925 cm^{-1} and 2954/2960 cm^{-1} (Fig. 2a–c). Residual plots were used to confirm the differences observed. For the highest electric field stress applied (11×10^5 Vm^{-1}), bands at 401 cm^{-1}, 813/845 cm^{-1}, 977 cm^{-1}, 1156/1171 cm^{-1}, 1332 cm^{-1}, 1439/1461 cm^{-1}, 2728 cm^{-1}, 2841 cm^{-1}, 2868/2885/2906 cm^{-1} and 2954/2960 cm^{-1} as well as a shoulder at 180 cm^{-1} seem to stand out (Fig. 3a–c). Except for the small shoulder, the same bands are indicated in both difference and residual data. However, it should be noted that when using a signal to noise ratio of 3:1 as the limit of detection, these peaks are not observed in every spectrum and therefore, further statistical analysis was employed.

PCA was employed to determine if the variance in difference and residual data can be used to determine if PP is under electric field stress, and which bands contribute to this separation to confirm the findings from the difference and residual data. It should be noted that PCA on spectroscopic data is only effective when noise within the spectra is kept to a minimum, otherwise even principal components with high eigenvalues will only describe noise [23]. Therefore, for the analysis presented in this paper only carefully selected regions of interest were considered, namely 200-550 cm^{-1}, 780-1475 cm^{-1}, 2700-2975 cm^{-1} weighted equally. It was also found that when the raw data was used for the PCA analysis, only a tentative separation the blocks could be achieved, with Block 1 ($a = 2$ mm) having a negative and Block 2 ($a = 5$ mm) having a positive principal component 1 score. This may be because, in the raw datasets, more background was considered for the PCA analysis than for difference and residual datasets. Hence, the difference and residual data were employed for further analysis to avoid this issue.

Score plots of principal component 1 versus principal component 2 for the Raman spectra in the 200-550 cm^{-1}, 780-1475 cm^{-1}, 2700-2975 cm^{-1} regions for differential and residual data are shown in Fig. 4 a and b respectively. In this figure, the PP samples are classified into two groups; charged and non-charged PP with only a few outliers of low charged PP within the non-charge group visible. In the difference data, charged samples generally exhibit a principal component 2 above 0 and a principal component 1 below 0, whereas non-charged samples show a principal component 2 below 0 and a principal component 1 above 0. For the residual data, charged samples exhibit a negative principal component 1, whereas non-charged PP show a positive principal component 1 value.

The PCA loadings plots of principal component 1 and principal component 2 for the difference and residual data are depicted in Fig. 4 c and 4 d respectively. When examining the loading plots, it can be seen that values of 401 cm^{-1}, 813/845 cm^{-1}, 977 cm^{-1}, 1156/1171 cm^{-1}, 1332 cm^{-1}, 1439/1461 cm^{-1}, 2841 cm^{-1}, 2868/2885/2906 cm^{-1} and 2954/2960 cm^{-1} seem to contribute to the principal components the most, especially to principal component 2. This principal component appears to be primarily responsible for the separation of charged and non-charged PP (Fig. 4a). Even data that initially failed to indicate significant differences in the difference plots with a signal to noise ratio of 3:1 appear to cluster using PCA analysis. Further, using PCA, data analysis of a large dataset, such as presented in this study, was able to establish a trend quickly and with equivalent results to the individual analysis of the difference plots.

Table 1
Main Raman bands affected by electric field. Conformation sensitive bands (chain conformation and configuration) are italic, bands with non-crystalline phase contribution bold; ν = stretching, ρ = rocking, σ = bending, τ = twisting, ω = wagging, b = backbone vibrations, sym. = symmetric, asym. = asymmetric [15].

Wavenumber m^{-1})	Main Active Group Vibration	Indicated Changes
401	*ωCH_2, σCH*	*Conformational Order, Unit Cell expansion*
813	***ρCH_2, νCC_b, $\nu C\text{-}CH_3$***	***Conformational Order***
845	ρCH_2, νCC_b, $\nu C\text{-}CH_3$	Conformational Order
977	**ρCH_3, νCC_b**	**Lamellae Orientation**
1156	**ρCH_3, νCC_b, $\nu C\text{-}CH_3$, σCH**	Conformational Order
1171	ρCH_3, νCC_b, σCH	Conformational Order
1332	**σCH, τCH_2**	**Interchain distance, Unit Cell expansion**
1439	**σCH_3 asym.**	**Unit Cell expansion**
1461	**σCH_3 asym., σCH_2**	
2841	**νCH_2 sym.**	**Smectic Modification,**
2868	**νCH_2 sym.**	**Molecular Orientation**
2885	**νCH_3 sym.**	
2906	**νCH_2 asym.**	
2925	**νCH_2 asym.**	
2954	**νCH_3 asym.**	
2960	**νCH_3 asym.**	

5. Discussion

5.1. Structural changes deduced from Raman data

5.1.1. Bands between 800 and 1200 cm^{-1}

Due to coupled modes, the bands between 800 and 1200 cm^{-1} can be used to determine the distribution of conformations. These bands are attributed to the 3_1 helix, which is the regular conformation in all iPP polymorphs, as well as the mesomorphic phase [16].

Both difference and residual data highlighted the importance of the 813/845 cm^{-1} bands when differentiating the charged and non-charged PP. In general, the region around 830 cm^{-1} is associated with molecular structure and orientation, as well as conformational defects, and the band at 813 cm^{-1} is often attributed to the amorphous structure. Indeed, it may not appear in any normal coordinate analysis of long ordered chains [5,24].

The content of PP macromolecules in the helical conformation with a significant number of conformational defects in the non-crystalline phase is indicated by the intensity ratio:

$$C_{helic} = \frac{I_{845}}{I_{813} + I_{830} + I_{845}} \quad \text{(Equation 3)}$$

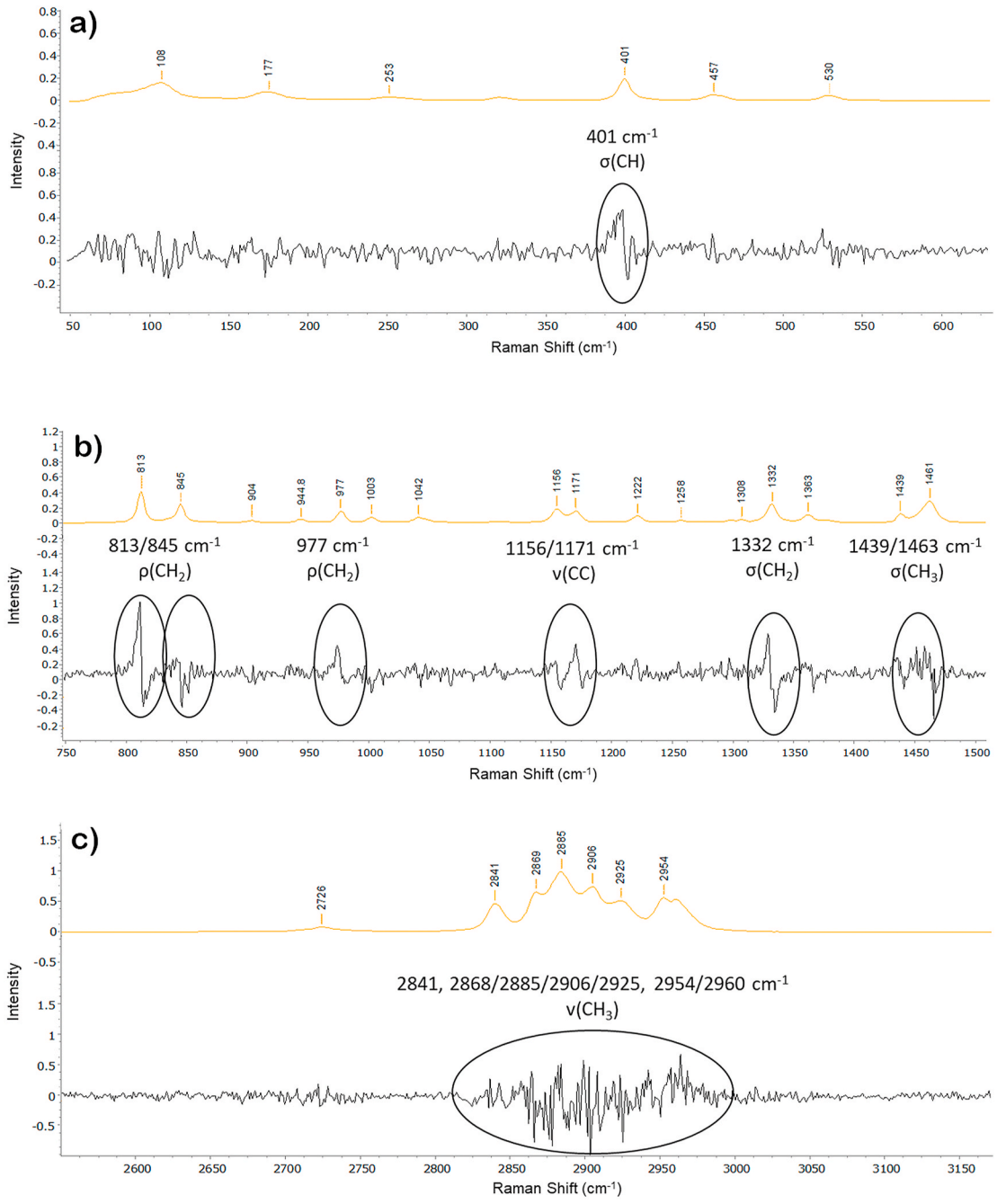

Fig. 2. Example difference plots for charged PP over 400-650 cm^{-1} (a), 750-1500 cm^{-1} (b) and 2550-3175 cm^{-1} (c). A PP Raman spectrum as reference is given for all ranges.

where I_{813}, I_{830}, and I_{845} are the integral intensities of the lines at 813 cm^{-1}, 830 cm^{-1}, and 845 cm^{-1}, respectively [25]. No prominent shoulder or peak at 830 cm^{-1} can be identified in our spectra however, indicating that the amount of atactic chains and therefore atactic PP present in the polymer tested is insignificant [26].

From the observed changes in the Raman spectra it can be seen that the helical conformation within the polymer is affected by the applied field. The assumption can be made that due to the change in vibrational motion, especially at the C–H bonds, the helix chains are transformed into more elongated trans conformations, similar to what occurs in helix conformational polymers under tensile stress. The transformation to the elongated trans conformations relieves stress and the distribution of stressed chains for the polymer decreases [27,28]. In general, helical conformation seems to decrease in iPP under stress. Bands containing significant contributions from backbone skeletal stretching are also sensitive to changes in chain conformation, which is indicated both in wavenumber and intensity changes.

The 813/845 cm^{-1} doublet is also an indicator of crystallinity, similar to the 1156/1171 cm^{-1} doublet [29]. In literature, the 1156/1171 cm^{-1} doublet is associated with chain stretching modes along with significant contributions from stretching and rocking modes [30–32]. The 1171 cm^{-1} band mainly consists of the crystalline phase, whereas that at 1156 cm^{-1} has been suggested to mainly originated from the amorphous phase [16]. The large contribution from axial stretching of the C–C backbone within the 1171 cm^{-1} band has previously been shown to have the highest sensitivity for other types of stress such as tensile stress. However, sensitivity varies with morphology, stress level and temperature and in this study, the band at 813 cm^{-1} is shown to be

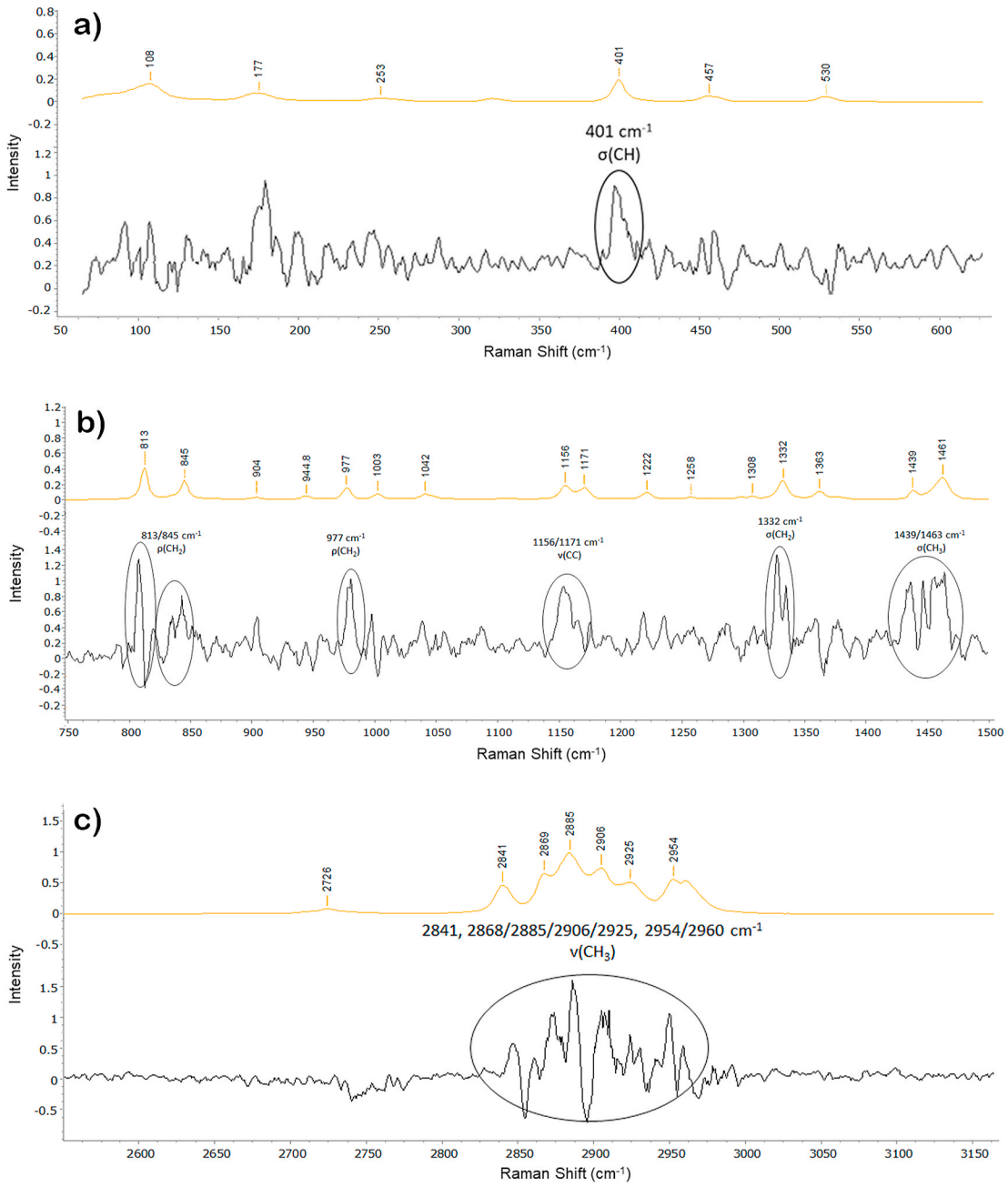

Fig. 3. Example residual plots for charged PP over 400-650 cm^{-1} (a), 750-1500 cm^{-1} (b) and 2550-3175 cm^{-1} (c). A PP Raman spectrum as reference is given for all ranges.

more affected by the electric field bias than 1171 cm^{-1} [16,33]. Both the band at 813 cm^{-1} and other bands such as at 1156 cm^{-1} are attributed with the amorphous phase and hence, the assumption can be made that the conformational changes occur more within the non-crystalline phase than within the crystalline structure and increase long range order.

The intensity ratio of the 977 cm^{-1} and 1003 cm^{-1} bands is also often used to assess molecular orientation and crystallinity [5]. In helix segments with at least 11 repeat units, the bands at 1003 cm^{-1} and 845 cm^{-1} are observed, with the band at 977 cm^{-1} attributed to shorter helix segments [16]. The intensity ratio of 977 cm^{-1} to 998 cm^{-1} has also been used as a Raman criterion of the lamellae orientation of iPP [34]. A change in lamellae orientation due to the applied electric field may explain the change within the 977 cm^{-1} band.

5.1.2. *Bands 401 cm^{-1} and 1332 cm^{-1}*

The bands at 401 cm^{-1} and 1332 cm^{-1} are related to the structural changes in the parallel and perpendicular directions of the molecule chain axis in the solid state. Both of these bands have two contributions, one sharp peak (crystalline component) and a weak broad band (amorphous component). Since the crystallinity of iPP at room temperature is quite high, the amorphous band is too weak to separate. However, peak position shifts in the crystalline band component of these bands can be interpreted as expansion within the unit cell, similar to thermal processes [10,35].

When looking at the fitted peak positional data of both bands, these tend to shift towards higher wavenumbers for 401 cm^{-1} and lower wavenumbers for 1332 cm^{-1} (Table 2). The 401 cm^{-1} band is also sensitive to conformational disorder and is essentially reproduced by skeletal vibration, where the hydrogen motions are omitted in the

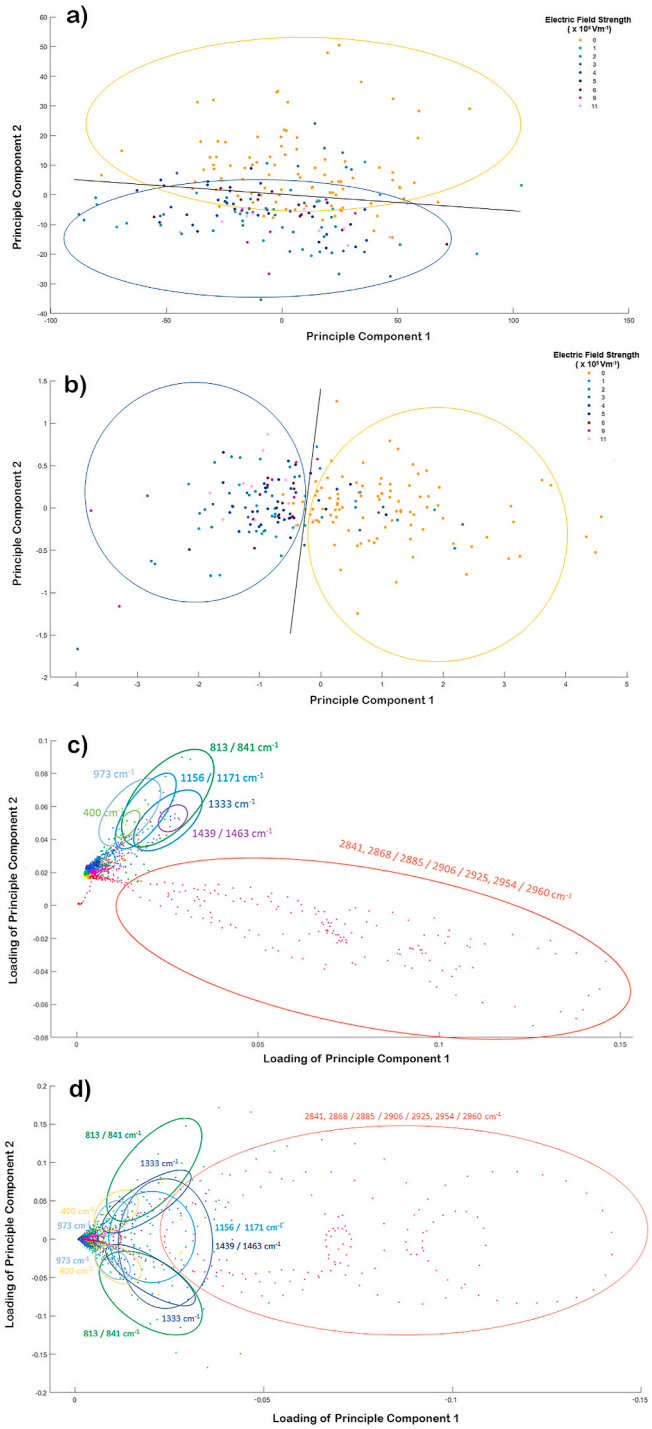

Fig. 4. PCA of Raman data. a) PCA clustering of difference Raman spectra, yellow circle corresponding to non-charged and blue circle to charged PP samples b) PCA clustering of residual Raman spectra, yellow circle corresponding to non-charged and blue circle to charged PP samples c) Principal Component 1 vs Principal Component 2 loading of the difference Raman data d) Principal Component 1 vs Principal Component 2 loading of the residual Raman spectra.

calculation [36,37]. With higher temperatures, the 401 cm^{-1} band has been shown to shift to higher wavenumbers, indicating changes within the crystalline structure as well as stretching along the chain axis [12]. A shift of this band to a higher wavenumber has also been attributed to the increase in the conformational disorder of the crystalline chains leading to an increase of the natural frequency of the coupled oscillators of the helical chain, which is similar to the disordered longitudinal acoustic mode [38]. This interpretation is also consistent with normal coordinate analysis [36], which predicts that helical chains shorter than 6 monomer units (2–3 complete turns in the helix) give a shoulder peak slightly above 401 cm^{-1} [35–37,39]. Sometimes, this shoulder is also interpreted as being representative of conformational defects within the macromolecular structure of the polymer [37,39]. It is likely that the distortion of the crystalline stems is closely related to the decrease of the helical sequences in this case. Similarly, a shift in wavenumber for the 1332 cm^{-1} band can be interpreted as a promotion of the twisting motions of the CH_2 groups due to increase in the inter-chain distance owing to expansion of the a*b plane [35]. Both the wavenumber of the peak maximum and the half-peak width of 1332 cm^{-1} decreases when the local strain increases, and the band changes its contour from asymmetrical to symmetrical. A small wavenumber shift of the band has been shown before for bulk iPP with its spherulitic structure deformed at room temperature [40–42].

A shift in the wavenumber of the 401 cm^{-1} and 1332 cm^{-1} bands as discussed here would indicate that the conformational disorder and the interchain distance increase at the molecular level. This may be explained by the anisotropy of the interactions between the parallel and perpendicular directions with respect to the chain axis. The van der Waals interactions in the interchain direction are likely to weaken with the increase of the interchain distance due to electric field stress and its expansion effects, whereas the covalent bonds of the polymer chain are less affected after a sufficiently random conformation is attained upon the application of the stress [35].

5.1.3. *Bands at 1439/1461 cm^{-1}*

These bands have been associated with several different vibrational modes. The doublet at 1439/1461 cm^{-1} has been assigned to the CH_2 scissoring. The band at 1461 cm^{-1} is attributed to CH_2 bending in the crystalline phase and the band at 1439 cm^{-1} to the CH_2 bending of the host polymer segments in the amorphous phase [33,43]. Interestingly, the 1439 cm^{-1} band often seems unaffected by polarisation geometry, showing little sensitivity to induced molecular orientation. The band at 1461 cm^{-1} also only seems to be slightly affected by chain deformations in uniaxially stretched iPP [40]. However, these bands have been shown to be sensitive to environmental changes, such as temperature variations [44]. Peak shifts at higher temperatures are assumed to be due to the expansion of the unit cell upon heating as well as an increase in number of defects in the crystalline region, which affects the environment of the vibrating groups and therefore the frequency. This results in an increasing disorder in the environment of the individual chains causing peak broadening [10,45]. Similar effects may take place with the electric field stress. This hypothesis of expansion of the unit cell is also supported by the shifts within the 401 cm^{-1} and 1332 cm^{-1} bands.

5.1.4. *Bands in the CH stretching region*

The bands between 2700 and 3000 cm^{-1} are not often used in quantitative structural analysis of PP, as a strong overlap of numerous broad bands exists in this region, and generally CH_2 stretching vibrations have not been found to be good indicators for stress level in other polymers such as polyethylene [11,39]. However, position and intensities of CH_3 stretching bands are especially sensitive to chain packing and are used for example to study β-α transitions [16]. Since phase transitions among polymorphs have been shown to be possible with changes in environmental factors such as an increase in temperature, a subtle difference noted between the Raman spectra could be related to these inter molecular interactions. However, these environmental changes have been shown to be more drastic than those expected to be experienced by the PP with applied electric field stress. Instead, it is more likely that the smectic phase of iPP is modified due to the electric field. This is mostly indicated by changes in the CH_2 and CH_3 stretching vibrations (2700-300 cm^{-1}) and in the spectral range around 800 cm^{-1}. The smectic state can be considered as an intermediate state between the

Table 2
Main Raman bands affected by the electric field and their shift in their fitted peak position with applied electric field strength. Standard deviation is given for uncertainty.

Peak position (cm^{-1}) at 0 Vm^{-1}	Relative peak shift (cm^{-1}) at different applied electric field strengths (x 10^6 Vm^{-1})							
	1	2	3	4	5	6	9	11
400.86±0.63	0.30	−0.40	0.34	−0.30	0.24	0.20	0.82	0.82
	±0.21	±0.55	±0.34	±0.63	±0.49	±0.40	±0.19	±0.22
812.33±0.45	0.25	−0.39	0.30	−0.25	0.21	0.22	0.54	0.70
	±0.20	±0.47	±0.36	±0.68	±0.66	±0.49	±0.21	±0.31
844.56±0.55	0.01	−0.44	0.07	−0.40	0.40	0.07	0.58	0.66
	±0.70	±0.75	±0.82	±0.71	±0.47	±0.78	±0.39	±0.46
977.14±0.51	0.28	−0.37	0.32	−0.95	0.18	0.18	0.48	0.53
	±0.20	±0.46	±0.35	±0.73	±0.64	±0.42	±0.37	±0.46
1155.26±0.49	0.31	−0.35	0.26	−0.22	0.18	0.43	0.39	0.52
	±0.20	±0.36	±0.35	±0.36	±0.38	±0.43	±0.19	±0.46
1170.72±0.51	0.25	−0.43	0.29	−0.26	0.17	0.20	0.36	0.48
	±0.22	±0.26	±0.34	±0.39	±0.38	±0.42	±0.17	±0.34
1332.36±0.48	−0.06	0.04	0.02	−0.13	−0.23	−0.33	−0.65	−0.81
	±0.16	±0.16	±0.25	±0.39	±0.34	±0.36	±0.13	±0.16
1438.38±0.50	0.29	−0.37	0.24	−0.25	0.19	0.25	0.27	0.54
	±0.18	±0.63	±0.37	±0.72	±0.63	±0.44	±0.14	±0.39
1461.43±0.49	0.27	−0.39	0.23	−0.24	0.16	0.19	0.23	0.48
	±0.18	±0.64	±0.35	±0.70	±0.62	±0.43	±0.19	±0.36
2841.46±0.23	−0.09	0.00	−0.07	−0.04	−0.03	0.10	0.00	−0.03
	±0.23	±0.22	±0.30	±0.33	±0.20	±0.10	±0.12	±0.25
2868.23±0.50	−0.01	0.05	0.15	0.09	0.14	0.31	−0.14	−0.13
	±0.36	±0.47	±0.36	±0.47	±0.19	±0.22	±0.44	±0.52
2885.42±0.52	−0.01	0.09	0.05	0.04	0.10	−0.05	−0.14	−0.08
	±0.37	±0.47	±0.35	±0.52	±0.28	±0.72	±0.53	±0.50
2905.54±0.51	−0.02	0.01	0.18	0.07	0.14	0.20	−0.07	−0.07
	±0.37	±0.44	±0.40	±0.50	±0.31	±0.24	±0.38	±0.58
2924.94±0.54	0.08	−0.03	0.25	0.04	0.21	−0.12	−0.11	−0.12
	±0.31	±0.49	±0.40	±0.68	±0.19	±0.58	±0.33	±0.56
2954.19±0.60	0.16	0.08	0.03	0.01	−0.12	0.09	−0.10	−0.13
	±0.61	±0.44	±0.46	±0.46	0.40	±0.54	±0.69	±0.66
2959.79±0.65	−0.59	0.18	0.01	−0.14	0.04	0.40	0.52	0.17
	±0.55	±0.45	±0.59	±0.76	±0.45	±0.40	±0.75	±0.47

amorphous and the crystalline phase, where the 3_1 helices are present, but with a disordered packing of the chains perpendicular to their axis. Especially bands at 2962 cm^{-1} and 2953 cm^{-1}, which correspond to the asymmetric stretching vibrations of the CH_3 group, have been shown to be affected by the smectic modification of PP [46]. In addition this doublet has been found to be indicative of change in molecular orientation [5,16]. Furthermore, intensities of the bands at 2841 cm^{-1}, 2868 cm^{-1} (symmetric stretching vibration of the CH_2 groups), 2906 cm^{-1} (CH stretching vibration), and 2925 cm^{-1} (asymmetric stretching vibration of the CH_2 groups) have been shown to increase with smectic modification [46].

5.2. Macrostructural and microstructural effects

The clustering of the Raman results indicate that the spectral changes observed when PP is electrically stressed, and the physical processes described above, are fully reversible i.e. no hysteresis was observed. When zero measurements are taken after an applied voltage, no difference between this measurement and a measurement taken before the bias can be seen. Further, all zero measurements seem to cluster close together as evident in the PCAs (Fig. 4a and b). Therefore, the stress does not exceed the elastic limit. Understanding these short-lived effects is important to better assess where faults and defects may occur within the material.

Almost all Raman bands of interest have a non-crystalline phase contribution. Bands whose non-crystalline phase contribution is negligible such as 401 cm^{-1}, 845 cm^{-1} and 1171 cm^{-1} are instead conformation sensitive bands, indicating a change in chain conformation within the polymer [25].

The macromolecular structure of polymers is often based on stacks of several lamellae running parallel and forming clusters. Indeed, in PP, lamellae units containing 3–10 lamellae crystals are present, which normally act together as one unit during deformation processes [47]. As the non-crystalline phase is affected most by the electric field stress, vibrational motion and changes in conformation likely occurs within the tie molecules, or junction points, connecting the overall cluster network. Minute stretching, caused by the electric field stress, also contributes to the slip and rearrangement within the crystal lamellae itself, eventually affecting the crystallinity and the crystal size of PP. More nucleation sites are able to form, and the number of crystals increase within the PP matrix. When the spherulite lamellae are induced during stretching, the spherulites break to form oriented cylindrite nuclei. Random molecular chains grow on the surface of the cylindrite nucleus and the electric field seems to promote the orientation of these molecular chains, similar to what can be observed in mechanical stresses. Helices misalign due to the stress, and amorphous molecular chains in the spherulites orient and form into a smectic mesophase near the yield point. This partially ordered mesophase of stable cylindrites reverts back to normal when the stress is removed [7,42,48]. In this elastic deformation stage, more orientated molecular chains along the stretching direction have now emerged between neighbouring lamellae. The insertion of an orientated structure counteracts the increase in the average distance between adjacent lamellae. Furthermore, this increase of number of crystals facilitates the transfer of stress and heat along the PP sheet [7].

The change in molecular orientation under electric stress is often seen in conjunction with the helix being deformed into a more elongated trans-like form [7,42,48]. Within the microscopic structure, shifts in the fitted peak position due to applied stress, especially those with high contributions of skeletal vibrations, have previously been interpreted in terms of the different average orientation accompanied by some degree of backbone chain deformation [41]. Some shifts can be observed in our dataset (Table 2), however the uncertainty associated with the peak position results in difficulty when concluding trends in most bands. The deformation of PP due to the electric field gives rise to changes in bond

stretching and angles as well as helical uncoiling or opening (torsional angle changes) discussed previously [42]. Intermolecular bonds transfer stress from one segment to the other. With stresses such as temperature, these bonds eventually rupture, and the stress distribution changes and segment mobility increases. Due to the reversible stress applied here, it is unlikely that a considerable number of permanent ruptures occur during the application of an electric field stress, however even a small number would reduce the overall lifetime of a polymer and its breakdown field strength [49].

The variation in microstructure would also include a work component, in which the deformation of the polymer chains is transferred into heat, resulting in a higher entropy. The electric field strength as well as the rate of a change in polarisation are important here. Specifically, dipole entities coupled to the electric field or dipole order parameter change due to the electric field. These changes in the dipole order thus change the dipole subsystem entropy, resulting in a slight temperature change, shown with dielectrics under electric field stress before [50–52]. This minor heat generation increases the mobility of the chains and therefore, allows for a better reorganisation and transformation of the polymer. This in turn changes crystalline modification and orientation [53]. The effect of entropy change in iPP due to the electric field is also less prominent due to the bulk nature of the material and therefore effects such as previously described electrically-enhanced thermally-induced bond scission and crack growth could not be described in this study, but may be a major factor in thin films [8].

6. Conclusion

This preliminary study investigated the effect of electric field stress on bulk polypropylene under normal environmental conditions using a non-invasive spectroscopic technique.

The non-crystalline phase appeared to be affected most by the electric field stress, showing that the vibrational motion and changes in conformation occur mostly within the tie molecules, connecting the overall cluster network. Specifically, helices misaligned due to the stress, and amorphous molecular chains in the spherulites oriented and formed into a smectic mesophase near the yield point. Slip and rearrangement of the crystal lamellae are also affected and eventually the crystallinity and the crystal size of iPP is changed. Particularly, orientated molecular chains are expected to form along the stretching direction between neighbouring lamellae. The insertion of an orientated mesophase structure counteracts the increase in the average distance between adjacent lamellae. These conformational defects can be seen across the macromolecular structure, increasing the interchain distances on the molecular level. This increase of crystals facilitates the transfer of stress along the PP sheet.

All these effects were reversable once the electric stress was removed. Long lasting effects from a very small number of ruptured overstressed segments could be possible but were not seen experimentally in this study. Overall, this study showed that the applied stress results in an electromechanical response in the polymer starting at the micro- and macromolecular level. With increased aging time, these changes may lead to adverse structural changes. Thus, in the future information on micro- and macrostructural changes may further be used to inform faults and defect detection within polymeric dielectric materials.

Data availability statement

The raw/processed data required to reproduce these findings cannot be shared at this time due to legal or ethical reasons.

CRediT authorship contribution statement

Marleen Vetter: Conceptualization, Methodology, Software, Data curation, Formal analysis, Validation, Investigation, Writing - original draft, Visualization. **Matthew J.F. Healy:** Supervision, Writing - review & editing. **David W. Lane:** Conceptualization, Supervision, Writing - review & editing.

Declaration of competing interest

The authors declare the following financial interests/personal relationships which may be considered as potential competing interests:

Acknowledgements

This work was supported by AWE and Cranfield University. We thank Karl Norris, Cranfield University, for his assistance in constructing the polypropylene test pieces. UK Ministry of Defence © Crown Owned Copyright 2020/AWE.

Appendix A. Supplementary data

Supplementary data to this article can be found online at https://doi.org/10.1016/j.polymertesting.2020.106851.

References

[1] J.P. Jones, J.P. Llewellyn, T.J. Lewis, The contribution of field-induced morphological change to the electrical aging and breakdown of polyethylene, IEEE Trans. Dielectr. Electr. Insul. 12 (5) (2005) 951–966, https://doi.org/10.1109/TDEI.2005.1522189. Available at:.

[2] P. Conner, J.P. Jones, J.P. Llewellyn, T.J. Lewis, A mechanical origin for electrical ageing and breakdown in polymeric insulation. ICSD'98, in: Proceedings of the 1998 IEEE 6th International Conference on Conduction and Breakdown in Solid Dielectrics (Cat. No.98CH36132, IEEE, 1998, pp. 434–438, https://doi.org/10.1109/ICSD.1998.709318. Available at:.

[3] T.P. Jones, T.J. Lewis, J.P. Llewellyn, Field-induced changes in the viscoelastic properties of polyethylene, in: Proceedings of the 2004 IEEE International Conference on Solid Dielectrics, ICSD 2004. IEEE, 2004, pp. 284–287, https://doi.org/10.1109/ICSD.2004.1350346, 2004, Available at:.

[4] G.G. Raju, Dielectrics in Electric Fields, 2st edn., CRC Press, Boca Raton, 2016.

[5] R. Heintz, M. Wall, D. Wieboldt, T.F. Scientific, Observing Molecular Orientation in Isotactic Polypropylene Films with Polarized Raman Spectroscopy, 2016.

[6] M. Slouf, E. Pavlova, S. Krejcikova, A. Ostafinska, A. Zhigunov, V. Krzyzanek, et al., Relations between morphology and micromechanical properties of alpha, beta and gamma phases of iPP, Polym. Test. 67 (March) (2018) 522–532, https://doi.org/10.1016/j.polymertesting.2018.03.039. Available at:.

[7] H. Ji, X. Zhou, X. Chen, H. Zhao, Y. Wang, H. Zhu, et al., Effects of solid-state stretching on microstructure evolution and physical properties of isotactic polypropylene sheets, Polymers 11 (4) (3 April 2019) 618, https://doi.org/10.3390/polym11040618. Available at:.

[8] P. Connor, J.P. Jones, J.P. Llewellyn, T.J. Lewis, Electric field-induced viscoelastic changes in insulating polymer films, in: 1998 Annual Report Conference on Electrical Insulation and Dielectric Phenomena (Cat. No.98CH36257), IEEE, 1998, pp. 27–30, https://doi.org/10.1109/CEIDP.1998.733842. Available at:.

[9] D.A. Strubbe, E.C. Johlin, T.R. Kirkpatrick, T. Buonassisi, J.C. Grossman, Stress effects on the Raman spectrum of an amorphous material: theory and experiment on a -Si:H, Phys. Rev. B Condens. Matter 92 (24) (2015) 1–6, https://doi.org/10.1103/PhysRevB.92.241202. Available at:.

[10] A. Brookes, J.M. Dyke, P.J. Hendra, S. Meehan, The FT-Raman spectroscopic study of polymers at temperatures in excess of 200°C, Spectrochim. Acta Mol. Biomol. Spectrosc. 53 (13) (November 1997) 2313–2321, https://doi.org/10.1016/S1386-1425(97)00171-6. Available at:.

[11] R.P. Wool, R.S. Bretzlaff, B.Y. Li, C.H. Wang, R.H. Boyd, Infrared and Raman spectroscopy of stressed polyethylene, J. Polym. Sci. B Polym. Phys. 24 (5) (1986) 1039–1066, https://doi.org/10.1002/polb.1986.090240508. Available at:.

[12] K. Tashiro, S. Minami, Quasiharmonic treatment of infrared and Raman vibrational frequency shifts induced by tensile deformation of polymer chains. II. Application to the polyoxymethylene, J. Polym. Sci. B Polym. Phys. 30 (10) (1992) 1143–1155, https://doi.org/10.1002/polb.1992.090301009. Available at:.

[13] T. Kida, Y. Hiejima, K.H. Nitta, Molecular orientation behavior of isotactic polypropylene under uniaxial stretching by rheo-Raman spectroscopy, Express Polym. Lett. 10 (8) (2016) 701–709, https://doi.org/10.3144/expresspolymlett.2016.63. Available at:.

[14] L. Marsich, A. Ferluga, L. Cozzarini, M. Caniato, O. Sbaizero, C. Schmid, The effect of artificial weathering on PP coextruded tape and laminate, Elsevier Ltd, Compos. Appl. Sci. Manuf. 95 (2017) 370–376, https://doi.org/10.1016/j.compositesa.2017.01.016. Available at:.

[15] I. De Wolf, Raman spectroscopy : about chips and stress Raman spectrum of silicon, Raman Spectrosc. 2 (2003).

[16] E. Andreassen, Infrared and Raman spectroscopy of polypropylene, in: J. Karger-Kocsis (Ed.), Polypropylene: an A-Z Reference, Kluwer Publishers, Dordrecht, 1999, https://doi.org/10.1007/978-94-011-4421-6. Available at:.

[17] F.R. Aussenegg, M.E. Lippitsch, On the electric field dependence of Raman scattering, J. Raman Spectrosc. 17 (1) (1986) 45–49, https://doi.org/10.1002/jrs.1250170110. Available at:.

[18] M.L. Shand, E. Burstein, Electric field modulated Raman scattering in CdS, Surf. Sci. 37 (June 1973) 145–152, https://doi.org/10.1016/0039-6028(73)90312-9. Available at:.

[19] L.J. Brillson, E. Burstein, L. Muldawer, Raman observation of the ferroelectric phase transition in SnTe, Phys. Rev. B 9 (4) (1974) 1547–1551, https://doi.org/10.1103/PhysRevB.9.1547. Available at:.

[20] H. Gibhardt, J. Leist, G. Eckold, Influence of electric field and domain structure on the low-temperature Raman spectra of $SrTiO_3$. Materials Research Express 2, IOP Publishing, 2014, 015005, https://doi.org/10.1088/2053-1591/2/1/015005. Available at: 1.

[21] G. Socrates, Infrared and Raman Characteristic Group Frequencies: Tables and Charts, 3nd edn., Wiley, Chichester, UK, 2001.

[22] D. Meeker, Finite element method magnetics, Available at: http://www.femm.info/, 2018.

[23] X. He, Y. Liu, S. Huang, Y. Liu, X. Pu, T. Xu, Raman spectroscopy coupled with principal component analysis to quantitatively analyze four crystallographic phases of explosive CL-20, RSC Adv. Roy. Soc. Chem. 8 (41) (2018) 23348–23352, https://doi.org/10.1039/C8RA02189A. Available at:.

[24] S.L. Hsu, Raman spectroscopic studies of polymer structure, in: Z.V. Popović (Ed.), Raman Scattering in Materials Science, Springer-Verlag, Berlin Heidelberg, 2010, pp. 369–445, https://doi.org/10.1007/978-3-662-04221-2_11. Available at:.

[25] K.A. Prokhorov, G.Y. Nikolaeva, E.A. Sagitova, P.P. Pashinin, M.A. Guseva, B. F. Shklyaruk, et al., Raman structural study of melt-mixed blends of isotactic polypropylene with polyethylene of various densities, Laser Phys. 28 (4) (2018), https://doi.org/10.1088/1555-6611/aaa9f7. IOP Publishing, Available at:.

[26] A.S. Nielsen, D.N. Batchelder, R. Pyrz, Estimation of crystallinity of isotactic polypropylene using Raman spectroscopy, Polymer 43 (9) (2002) 2671–2676, https://doi.org/10.1016/S0032-3861(02)00053-8. Available at:.

[27] T. He, Polymer strength and chain conformation, Makromol. Chem. 188 (1987) 2489–2494, https://doi.org/10.1002/macp.1987.021881023. Available at:.

[28] J. Kang, J. Chen, Y. Cao, H. Li, Effects of ultrasound on the conformation and crystallization behavior of isotactic polypropylene and β-isotactic polypropylene, Polymer 51 (1) (2010) 249–256, https://doi.org/10.1016/j.polymer.2009.11.018. Elsevier Ltd, Available at:.

[29] G.V. Fraser, P.J. Hendra, D.S. Watson, M.J. Gall, H.A. Willis, M.E.A. Cudby, The vibrational spectrum of polypropylene, Spectrochim. Acta Mol. Spectros 29 (7) (July 1973) 1525–1533, https://doi.org/10.1016/0584-8539(73)80216-8. Available at:.

[30] G. Ellis, M.A. Gómez, C. Marco, Mapping the crystalline morphology of isotactic polypropylene by infrared microscopy, Int. J. Vibr. Spec. 5 (4) (2001) 7.

[31] R.G. Snyder, J.H. Schachtschneider, Valence force calculation of the vibrational spectra of crystalline isotactic polypropylene and some deuterated polypropylenes, Spectrochim. Acta 20 (5) (1964) 853–869, https://doi.org/10.1016/0371-1951(64)80084-9. Available at:.

[32] T. Miyazawa, Y. Ideguchi, K. Fukushima, Molecular vibration and structure of high polymers. IV. A general method of treating degenerate normal vibrations of helical polymers and infrared-active vibrations of isotactic polypropylene, J. Chem. Phys. 38 (11) (1963) 2709–2720, https://doi.org/10.1063/1.1733578. Available at:.

[33] T. Furukawa, M. Watari, H.W. Siesler, Y. Ozaki, Discrimination of various poly (propylene) copolymers and prediction of their ethylene content by near-infrared and Raman spectroscopy in combination with chemometric methods, J. Appl. Polym. Sci. 87 (4) (2003) 616–625, https://doi.org/10.1002/app.11351. Available at:.

[34] J. Martin, P. Bourson, A. Dahoun, J.M. Hiver, The β-spherulite morphology of isotactic polypropylene investigated by Raman spectroscopy, Appl. Spectrosc. 63 (12) (December 2009) 1377–1381, https://doi.org/10.1366/000370209790109067. Available at:.

[35] Y. Hiejima, K. Takeda, K.H. Nitta, Investigation of the molecular mechanisms of melting and crystallization of isotactic polypropylene by in situ Raman spectroscopy, Macromolecules 50 (15) (2017) 5867–5876, https://doi.org/10.1021/acs.macromol.7b00229. Available at:.

[36] T. Hahn, W. Suen, S. Kang, S.L. Hsu, H.D. Stidham, A.R. Siedle, An analysis of the Raman spectrum of syndiotactic polypropylene. 1. Conformational defects, Polymer 42 (13) (2001) 5813–5822, https://doi.org/10.1016/S0032-3861(00)00904-6. Available at:.

[37] V.M. Hallmark, S.P. Bohan, H.L. Strauss, R.G. Snyder, Analysis of the low-frequency isotropic Raman spectrum of molten isotactic polypropylene, Macromolecules 24 (14) (1991) 4025–4032, https://doi.org/10.1021/ma00014a009. Available at:.

[38] R.G. Snyder, The structure of chain molecules in the liquid state: low-frequency Raman spectra of n-alkanes and perfluoro-n-alkanes, J. Chem. Phys. 76 (8) (1982) 3921–3927, https://doi.org/10.1063/1.443508. Available at:.

[39] E.A. Sagitova, P. Donfack, G.Y. Nikolaeva, K.A. Prokhorov, P.P. Pashinin, P. M. Nedorezova, et al., New insights into the structure of polypropylene polymorphs and propylene copolymers probed by low-frequency Raman spectroscopy, J. Phys. Conf. 826 (1) (20 April 2017), 012006, https://doi.org/10.1088/1742-6596/826/1/012006. Available at:.

[40] J.C. Rodríguez-Cabello, J.C. Merino, T. Jawhari, J.M. Pastor, RheoOptical Raman study of chain deformation in uniaxially stretched bulk isotactic polypropylene, J. Raman Spectrosc. 27 (6) (June 1996) 463–467, https://doi.org/10.1002/(SICI)1097-4555(199606)27:6<463::AID-JRS979>3.3.CO;2-2. Available at:.

[41] Y. Song, K.H. Nitta, N. Nemoto, Molecular orientations and true stress-strain relationship in isotactic polypropylene film, Macromolecules 36 (21) (2003) 8066–8073, https://doi.org/10.1021/ma030194d. Available at:.

[42] J.M. Chalmers, M.W. Mackenzie, H.A. Willis, H.G.M. Edwards, J.S. Lees, D.A. Long, FTIR spectroscopic studies of isotactic polypropylene films under stress, Spectrochim. Acta Mol. Spectros 47 (12) (1991) 1677–1683, https://doi.org/10.1016/0584-8539(91)80005-4. Available at:.

[43] G.A. Voyiatzis, K.S. Andrikopoulos, Fast monitoring of the molecular orientation in drawn polymers using micro-Raman spectroscopy, Appl. Spectrosc. 56 (4) (2002) 528–535, https://doi.org/10.1366/0003702021954999. Available at:.

[44] G.Y. Nikolaeva, E.A. Sagitova, K.A. Prokhorov, P.P. Pashinin, P.M. Nedorezova, A. N. Klyamkina, et al., Using Raman spectroscopy to determine the structure of copolymers and polymer blends, J. Phys. Conf. 826 (1) (20 April 2017), 012002, https://doi.org/10.1088/1742-6596/826/1/012002. Available at:.

[45] R.M. Khafagy, In situ FT-Raman spectroscopic study of the conformational changes occurring in isotactic polypropylene during its melting and crystallization processes, J. Polym. Sci. B Polym. Phys. 44 (15) (1 August 2006) 2173–2182, https://doi.org/10.1002/polb.20891. Available at:.

[46] J.M. Chalmers, H.G.M. Edwards, J.S. Lees, D.A. Long, M.W. Mackenzie, H.A. Willis, Raman spectra of polymorphs of isotactic polypropylene, J. Raman Spectrosc. 22 (11) (1991) 613–618, https://doi.org/10.1002/jrs.1250221104. Available at:.

[47] K. Nitta, M. Yamana, Poisson's ratio and mechanical nonlinearity under tensile deformation in crystalline polymers, Rheology (2012), https://doi.org/10.5772/34881. Available at:.

[48] R.P. Wool, R.H. Boyd, Molecular deformation of polypropylene, J. Appl. Phys. 51 (10) (1980) 5116–5124, https://doi.org/10.1063/1.327429. Available at:.

[49] V.I. Vettegren, Novak II., Friedland KJ. Overstressed interatomic bonds in stressed polymers, Int. J. Fract. 11 (5) (1975) 789–801, https://doi.org/10.1007/BF00012897. Available at:.

[50] B. Neese, B. Chu, S.-G. Lu, Y. Wang, E. Furman, Q.M. Zhang, Large electrocaloric effect in ferroelectric polymers near room temperature, Science 321 (5890) (8 August 2008) 821–823, https://doi.org/10.1126/science.1159655. Available at:.

[51] H.H. Wu, R.E. Cohen, Polarization rotation and the electrocaloric effect in barium titanate, J. Phys. Condens. Matter 29 (2017) 485704, https://doi.org/10.1088/1361-648X/aa94db. Available at:.

[52] V.S. Bondarev, I.N. Flerov, M.V. Gorev, E.I. Pogoreltsev, M.S. Molokeev, E. A. Mikhaleva, et al., Influence of thermal conditions on the electrocaloric effect in a multilayer capacitor based on doped $BaTiO_3$, J. Adv. Dielectr. 7 (6) (2017) 1750041, https://doi.org/10.1142/S2010135X17500412. Available at:.

[53] J.M. Pastor, T. Jawhari, J.C. Merino, J. Fraile, Micro-Raman study of the transition front in uniaxially stretched semicrystalline polymers, Makromol. Chem. Macromol. Symp. 72 (1) (June 1993) 131–141, https://doi.org/10.1002/masy.19930720111. Available at:.